Composite Structures 155 (2016) 245–254

Contents lists available at ScienceDirect

Composite Structures

journal homepage: www.elsevier.com/locate/compstruct

Behavior of glass and carbon FRP tube encased recycled aggregate concrete with recycled clay brick aggregate

Chang Gao [a], Liang Huang [a,*], Libo Yan [b,c,*], Bohumil Kasal [b,c], Wengui Li [a,d]

[a] College of Civil Engineering, Hunan University, Changsha 410082, China
[b] Centre for Light and Environmentally-Friendly Structures, Fraunhofer Wilhelm Klauditz-Institut WKI, Bienroder Weg 54E, 38108 Braunschweig, Germany
[c] Department of Organic and Wood-Based Construction Materials, Technical University of Braunschweig, Hopfengarten 20, 38102 Braunschweig, Germany
[d] Department of Civil Engineering, Monash University, Clayton, Victoria 3800, Australia

ARTICLE INFO

Article history:
Received 30 March 2016
Revised 3 August 2016
Accepted 18 August 2016
Available online 19 August 2016

Keywords:
Recycle aggregate concrete
Recycled clay brick aggregates
Glass and carbon fibre-reinforced polymer (FRP)
Confinement models

ABSTRACT

In literature, there are few studies which investigated compressive behavior of fibre reinforced polymer (FRP) tube confined recycled aggregate concrete (RAC) where the recycled aggregates (RAs) mainly came from demolished old concrete components. Study which considered FRP tube confined RAC using recycled clay brick aggregates (RCBA) originating from demolished brick masonry components is rare. Thus, this paper reports a systematic study on axial compressive behavior of FRP tube encased RAC containing RCBA (termed as FRP-confined RAC-RCBA). The experimental variables considered are, i.e., replacement ratio of RCBA (r = 0, 50, 70 and 100%), FRP tube thickness (n_f = 2, 4 and 6 layers) and type of fibre material (GFRP and CFRP). This study shows that both GFRP and CFRP tubes enhanced strength and deformation of the confined RAC-RCBA specimens remarkably. The ultimate compressive stress of the confined specimens decreased with an increase of RCBA replacement ratio but their axial deformation kept approximately constant. Failure mode and the compressive stress-strain behavior of G/CFRP-confined RAC-RCBA were similar to these tube confined normal aggregate concrete (NAC) and the ultimate compressive strength of G/CFRP tube confined RAC-RCBA specimens enhanced with an increase in FRP tube thickness. The CFRP-confined specimens showed higher ultimate strength but lower ultimate axial strain than those of GFRP-confined specimens. The applicability of eight widely used confinement models, i.e., 5 design-oriented and 2 analysis-oriented models, for FRP-confined NAC to FRP-confined RAC-RCBA was also evaluated.

1. Introduction

In the last decades, large amounts of construction and buildings have been demolished in the worldwide and millions of tons of construction and demolition waste (CDW) have been generated [1,2]. The recycling of CDW emerged popularly to create the social, environmental significant and economic product, i.e. recycled aggregate concrete (RAC) [3]. Generally, natural aggregates (NAs) were collected by cutting mountains and breaking river gravels, which consumed huge amount of natural resources. It is believed that the use of RAC will be a great step to reduce the large depletion of natural resources [4]. On the basic of this, RACs have been studied and used but mainly limited for non-structural application (i.e. construction of landfills) [5–8] because for RAC made of recycled clay brick aggregate (RCBA), the aggregates with high water absorption and relatively low strength lead to the produced RAC with reduced stiffness and strength in comparison with concrete made of NAs [9,10]. However, the annual amounts of demolition brick waste are considerable [13] and more than 50% of demolition wastes consist of clay bricks or cement blocks in many countries [11–13]. Moreover, it is not only costly but also technically impossible to separate the clay bricks from the recycled aggregates (RAs) or original constructions, and a small amount of waste impurities will be still remained even after the tedious cleaning procedure, thus, the mixtures of RAs and RCBAs have to be considered for use without separation [14].

In literature, there are many studies which considered concrete with RAs from demolished concrete components and crushed clay bricks. It was reported that the mechanical properties of concrete with RAs from demolished concrete components and crushed clay bricks are highly influenced by parameters such as water

* Corresponding authors at: Centre for Light and Environmentally-Friendly Structures, Fraunhofer Wilhelm Klauditz-Institut WKI, Bienroder Weg 54E, 38108 Braunschweig, Germany (L. Yan).

E-mail addresses: lianghuanghnu@gmail.com (L. Huang), l.yan@tu-braunschweig.de (L. Yan).

http://dx.doi.org/10.1016/j.compstruct.2016.08.021
0263-8223/

absorption, water cement ratio, replacement ratio, shape and size of the RAs, impurities, and chemical composition of the RACs [4,10,14–16]. Studies showed that the reason for a low stiffness and strength of RAC using RCBA was attributed to the low compressive strength of original brick or rock, and the compressive strength of concrete produced with RCBA, which was only acceptable to be used in non-structural purpose [17]. It was also found that a 50% of RCBA replacement ratio led to a low workability of its RAC among various replacement ratios (i.e. 10%, 30%, 70% and 100%) and the cement mortar on attached aggregates had a significant effect on the mechanical properties of fresh and the hardened RAC [14]. Other research showed that the RAs with replacement ratio of 100% for both coarse and fine aggregate resulted in a 16% reduction in concrete strength compared with the natural aggregate concrete (NAC) counterpart [18,19]. Recent investigation also indicated a remarkable effect of water-cement ratio (ω/c) on the workability and strength of RAC, i.e. if the ω/c reduced from 0.55 to 0.40, the strength and Young's modulus of the RAC improved significantly [4]. Thus, the mechanical properties of RAC-RCBA need to be improved for better and wider applications, especially for structural concrete.

It is well known that use of confinement to concrete (e.g., steel tubes or stirrups, FRP tubes or wrappings) is an effective way to improve the mechanical properties of normal aggregate concrete (NAC) [20–29]. In a FRP tube confined NAC, i.e. the so called concrete filled FRP tube (CFFT), the pre-fabricated FRP tube serves as permanent formwork for fresh concrete and also provides confinement to the infilled concrete to enhance the strength and ductility of the structure [30,31]. Recently, the compressive behavior of CFFT has been investigated systematically, e.g. by Ozbakkaloglu's group [30–39]. The effects of various experimental parameters such as concrete strength [32,33], confinement method [32], slenderness [34], use of silica fume [35], fibre type [36], overlap configuration [37], fibre orientation [38], specimen end condition [38], and tube shape (i.e. square, rectangular and circular) [39] on the compressive behavior of CFFT have been well documented. All those studies indicated that FRP tube confinement can enhance the strength and ductility of NAC remarkably. On the basis of this, most recently some researchers considered to use FRP tube as confining material of RAC, e.g., Islam et al. [40], Xiao et al. [41] and Zhao et al. [42] and Xie and Ozbakkaloglu [43]. Xiao et al. [41] discussed the compressive behavior of RAC confined by GFRP tubes. The results indicated that both the strength and deformation of RAC were improved, while the confined concrete peak stress decreased with an increase in replacement ratio of RAs. Islam et al. [40] stated that the increase in axial compressive strength was 82% and 95% for RAC cylinders with CFRP and GFRP confinement, respectively. Zhao et al. [42] also showed that the use of FRP confinement improved the mechanical properties of RAC significantly. Xie and Ozbakkaloglu et al. [43] investigated the effects of RCA replacement ratio, specimen cross sectional shape, FRP type, and concrete strength on the compressive behavior of FRP tube confined RAC. However, it should be pointed out here that in these studies [40–43], the RAs used for the RAC came from demolished old concrete components, no RAs using recycled clay brick aggregate (RCBA) are considered for the confined RAC. If RCBA from demolished brick waste can also be used for structural concrete application, the concrete industry will be close to sustainability. Therefore, research is needed to understand the compressive behavior of FRP confined RAC containing RCBA.

On the basis of this, the compressive behavior of GFRP and CFRP tube encased RAC with different replacement ratios of RCBA were studied systematically in this study. The experimental variables considered included: (1) the replacement ratio of RCB coarse aggregates r (i.e. the mass fraction of the RCB coarse aggregates to the total mass of coarse aggregates), (2) the number of FRP layers n_f, and (3) the type of FRP material (CFRP and GFRP). In addition, the experimental results were compared with the predicted values based on the seven widely used confinement models developed for FRP-confined NAC.

2. Experiments

2.1. Unconfined plain RAC with RCBAs

In this study, the clay bricks used for RCBAs were generated from load bearing masonry walls, cladding and partition walls, and then manufactured as recycled clay brick aggregates through sorting and crushing process. The RCBAs were collected from Jinke Resource Recycling co. LTD in Henan Province, China, which were derived from a mixture of CDW with different strengths and ages. The RCBAs were screened manually and dried to keep same moisture content for concrete mixing, as illustrated in Fig. 1. To understand the mechanical properties of RAC with RCBAs (termed as RAC-RCBA), compressive strength test was carried out initially for normal plain concrete and the RAC. The test matrix of the RACs with different replacement ratios of RCBA is given in Table 1, where the NPCM denotes plain NAC cylinder with a diameter of 100 mm and a height of 200 mm, the PCA50M, PCA70M and PCA100M denote plain RAC with the RCBA replacement ratio of 50%, 70% and 100%, respectively and with the same size of NPCM, i.e. diameter of 100 mm and a height of 200 mm.

The relationship between compressive strength and replacement ratio of RCBA for unconfined plain RAC specimens is illustrated in Fig. 2. The axial and lateral stress-strain curves of NAC

Fig. 1. The recycled clay brick aggregates ($d = 5\sim10$ mm).

Table 1
Test samples of plain concrete.

Specimens	RCBA in coarse aggregate (%)	Water-cement ratio
NPCM	0	0.41
PCA50M	50	0.41
PCA70M	70	0.41
PCA100M	100	0.41

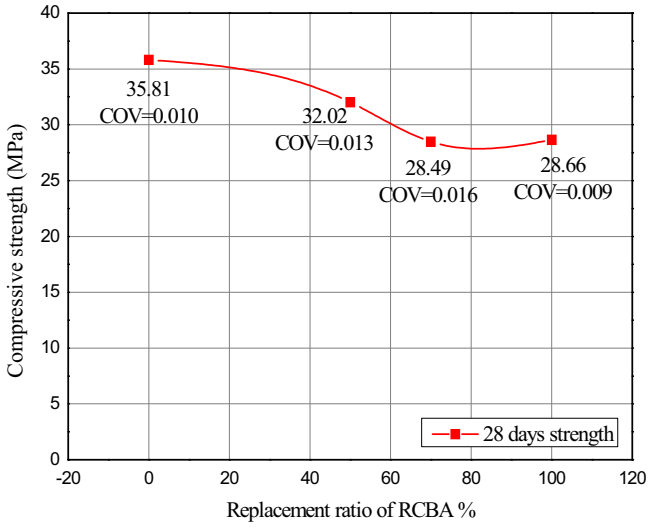

Fig. 2. Compressive strength of plain concrete of various replacement ratio.

and the RAC-RCBAs with four different replacement ratios of RCBAs (i.e., 0%, 50%, 70% and 100%) at 28-day with the same water-cement ratio are presented in Fig. 3. Fig. 2 shows that in general, an increase in replacement ratio of RCBA leads to a reduction in compressive strength of the RAC, i.e. 11.8% and 12.4% strength reduction among the RAC-RCBAs with the replacement ratio ranged from 0% to 50% and from 0% to 70%. There is no noticeable difference on the compressive strength between the RAC-RCBA specimen with a RCBA replacement ratio of 70% and that with the replacement ratio of 100%. Fig. 3 shows that both axial and hoop strain at the peak strength of all the RACs (with replacement ratios of 50, 70 and 100%) are slightly larger than the NAC counterparts. However, it is clear that the slope of the NAC is larger than that of the RACs with RCBA, indicating the reduction in stiffness of RAC due to the use of RCBAs. Fig. 4 shows the failure mode of RAC with different replacement ratios of RCBAs. It is clear that the general failure mode of all the RAC specimens is similar to that of NAC, but the RACs with RCBA illustrate more apparent explosion at the mid-height of the cylinders and show more vertical cracks compared with the NAC counterpart.

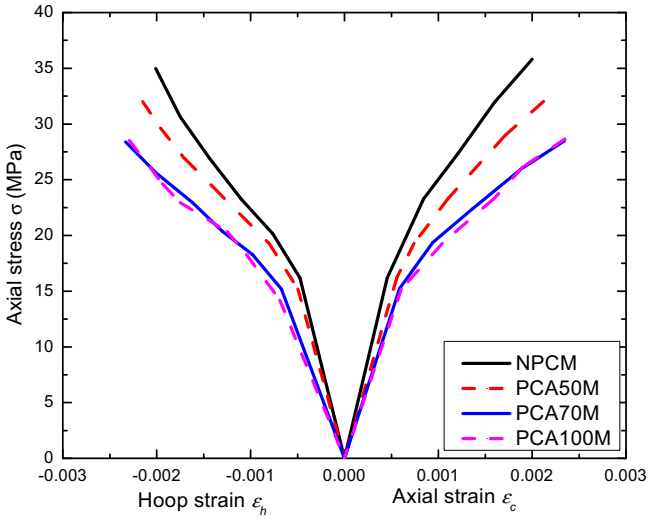

Fig. 3. Axial stress versus axial and lateral strains curves for unconfined RAC with various replacement ratios of RCBAs.

2.2. Raw materials and specimen preparations for FRP confined RAC-RCBA

To investigate the compressive behavior of FPR tube encased RAC-RCBA specimens, 39 cylindrical specimens (i.e. 27 FRP confined RAC-RCBA cylinders and 12 unconfined plain RAC-RCBA cylinders) were prepared. These specimens were classified into 9 categories of FRP-confined RAC-RCBA and 4 categories of control plain NAC and plain RAC-RCBA; each specimen category included three identical specimens. Three tested parameters were considered: (1) the replacement ratio of RCBAs r (i.e. the mass fraction of the RCB coarse aggregates to the total mass of coarse aggregates), (2) the number of the FRP layers n_f, and (3) the type of FRP materials (CFRP and GFRP). All concrete specimen groups casted with the same water-cement ratio, which was equal to 0.41 to ensure only one variable of each experimental group. The variation of FRP confinement stiffness was designed to use 2, 4 and 6 layers of GFRP and CFRP. The replacement ratios of RCBA

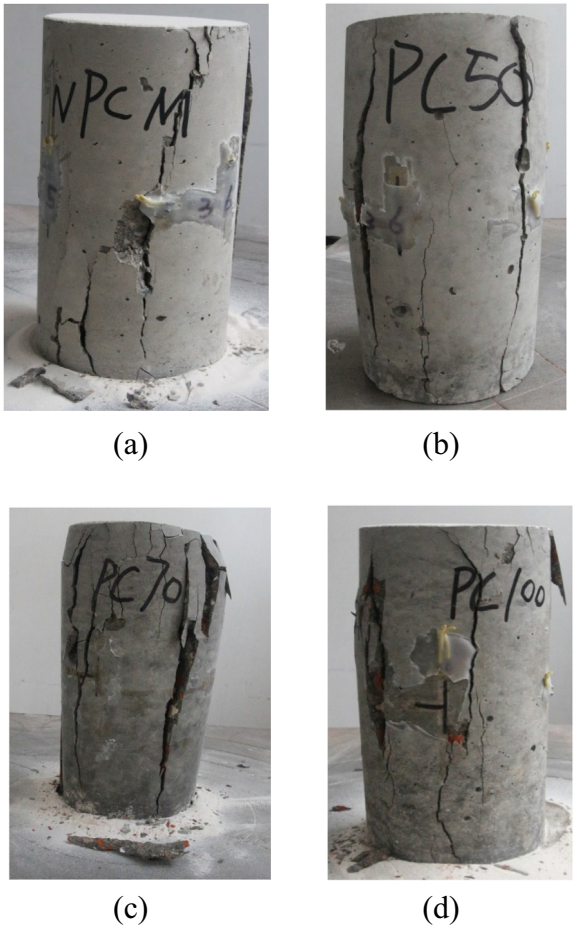

Fig. 4. Typical failure of plain concrete: (a) NAC, (b) PCA50M, (c) PCA70M, (d) PCA100M.

used for GFRP and CFRP tube confined RAC-RCBA was 0%, 50%, 70% and 100%.

The details of all the specimens are listed in Table 2, the letter *G* with a figure denotes the number of layers of GFRP tube, the letter *C* with a figure denotes the number of layers of CFRP tube, the letter *A* with a percentage denotes the replacement ratio of RCBA, specimen G4A70M is the GFRP-confined RAC-RCBA cylinder with the size ($D \times H = 100 \times 200$ mm), the tube thickness of 4 layer GFRP and the RCBA replacement ratio of 70%.

The mix proportions of NAC and the RAC-RCBA are listed in Table 3. Normal Portland cement (type I, 42.5 MPa) and river sand (with fineness modulus$M_K = 2.7$) were used for all specimens. Since the RCBAs were collected from demolished masonry structures made of clay bricks which had high water absorption, the moisture content and the water absorption of the RCBAs were tested and the results are given in Table 3. The water mass was also considered being adjusted to make sure the water-cement ratio was a constant by measuring the moisture content of the RCBAs. By doing so, the replacement ratio of RCBA was fixed as the sole variable of the RACs. The average compressive strength of the plain concrete with RCBA replacement ratios of $r = 0\%$, 50%, 70% and 100% was $f_{co} = 35.9$ MPa, 35.6 MPa, 33.3 MPa and 31.7 MPa, respectively and the corresponding strain at peak stress was $\varepsilon_{co} = 0.0027, 0.0026, 0.0028$ and 0.0030, respectively.

Unidirectional glass fabrics and plain weave bi-directional carbon fabrics were infiltrated into the epoxy resin to make these G/CFRP tubes with PVC tube as the mould. A thin layer of plastic film was covered on the PVC tube mould which was brushed with oil for an easy removal of the FRP tube from the PVC mould. For the GFRP tubes, the fibre direction was the hoop direction of the tube. For CFRP tubes, the fibre orientation was 90° along the longitudinal axis of the tube since the carbon fabric has a plain weave structure. The overlapping length of both G/CFRP tubes was one third perimeter of the concrete cylinder. The air bubble and additional epoxy were squeezed out during the fabrication. The FRP tubes were then dried and cured at room temperature for 7-day before demolded.

The tubes were placed on a smooth plate, then concrete was casted, poured and compacted by a vibrator. The cylinders were cured in the room temperature (20 ± 3) °C, covered by thermal insulation cloth and watered three times per day for 28 days [44]. Both ends of the G/CFRP tube confined specimens were strengthened by the corresponding G/CFRP sheet with a width of 2 mm and thickness of 5 layers of FRP to avoid premature cracking of the FRP tubes at the ends.

Table 2
Specimens Matrix.

Specimens	*D* (mm)	*H* (mm)	Type of FRP	FRP stiffness n_f	Replacement ratio of RCBA *r* (%)
G4A0M	100	200	G	4	0
G4A50M	100	200	G	4	50
G4A100M	100	200	G	4	100
G4A70M	100	200	G	4	70
G6A70M	100	200	G	6	70
G2A70M	100	200	G	2	70
C2A70M	100	200	C	2	70
C4A70M	100	200	C	4	70
C6A70M	100	200	C	6	70
PCA50M	100	200	–	–	50
PCA70M	100	200	–	–	70
PCA100M	100	200	–	–	100
NPCM	100	200	–	–	0

Table 3
Mix proportions of concrete with different replacement ratios of RCB.

Replacement ratio	*r* = 0%	*r* = 50%	*r* = 70%	*r* = 100%
Free Water (*kg*)	121	121	121	121
Water Content (*kg*)	9.8	9.8	9.8	9.8
Cement (*kg*)	296	296	296	296
Fine aggregate (*kg*)	280	280	280	280
RCB aggregate (*kg*)	–	284	398	568
Normal aggregate (*kg*)	568	284	170	–
Water-cement ratio ω/c	0.41	0.41	0.41	0.41

2.3. Test setup and instrumentation

For each specimen, three hoop strain gauges (SG1 to SG3) and three axial strain gauges (SG4 to SG6) were installed on the mid-height of the cylinders with 120° apart from each other to record the hoop and axial strains of the specimens, and two axial strain gauges (SG7 and SG8) were mounted at two ends of the cylinders to record the axial strain at the two ends of the tube, as illustrated in Fig. 5. The cylinders were tested under monotonic axial compression using a high-stiffness compression testing machine (with a capacity of 20,000 kN) using a displacement-control rate of 0.20 mm/min.

The axial displacement of the specimen was measured by four linear variable displacement transducers (LVDTs) at the four corners of the compression board of the testing machine. The whole loading process was executed by a controlled displacement rate of 0.20 mm/min until the failure of the cylinders. The longitudinal and transverse strains, loads and displacements were measured simultaneously.

2.4. Properties of FRP materials

Flat coupon tests were carried out to determine the tensile properties of G/CFRP composite materials according to ASTM D3039 [45]. For the flat coupon tensile testing, five coupons with width of 25 mm and length of 250 mm were cut along the fibre direction from the fabrics; four aluminum tabs of with a width of 30 mm and the length of 56 mm were tabbed on both ends of the FRP coupons to avoid premature failure of the coupon ends, as shown in Fig. 6. The tested results are given in Table 4, the tensile strength and modulus of CFRP was much larger than that of GFRP. The typical tensile stress-strain curves of FRP are shown in Fig. 7, it can be seen that both GFRP and CFRP laminates show a linear elastic behavior in tension.

3. Results and discussion

3.1. Failure mode

The typical failure modes of the tested specimens are shown in Fig. 8. The plain RAC-RCBA cylinder failed fragilely with one major vertical crack which was similar to that of the plain NAC cylinder. For the GFRP-confined RAC-RCBA cylinders, the failure occurred when the GFRP tube ruptured at the mid-height of the tube due to the lateral expansion of the core concrete. The GFRP tube failed with some apparent features, e.g. some discontinuous tearing sound, cracks emerged gradually and the FRP hunched gradually until the rupture of FRP in tension. The CFRP tube confined cylinders expressed a more brittle failure, occurred suddenly like an explosion with big sounds. There is no apparent difference in failure modes among these specimens with different replacement ratios of RCBA and materials of GFRP and CFRP, while the failure process of the confined RAC-RCBA with thicker FRP tube developed slower and the FRP tube ruptured more completely.

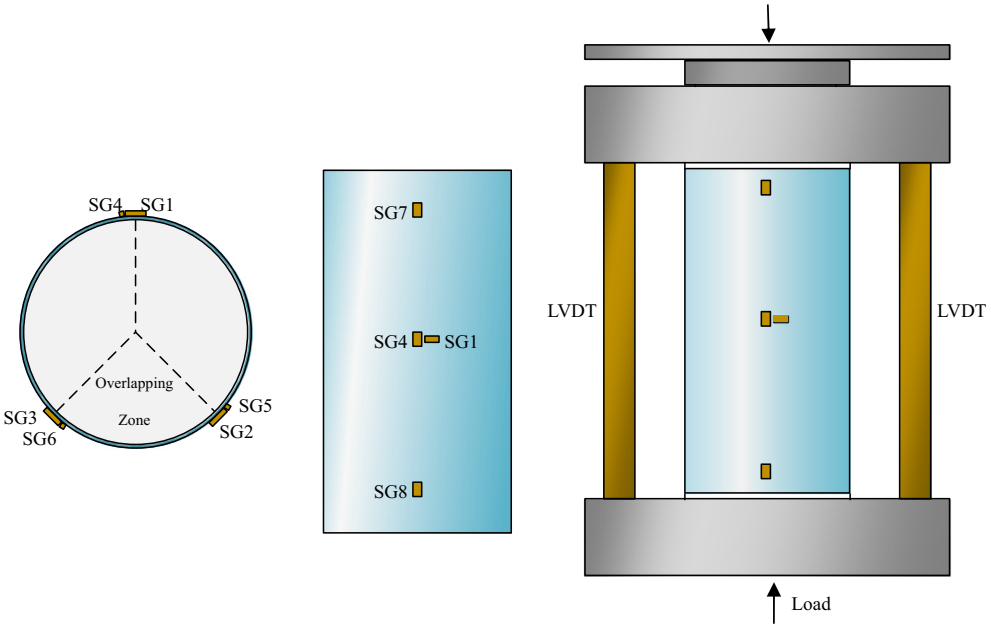

Fig. 5. Test setup and instrumentation configurations.

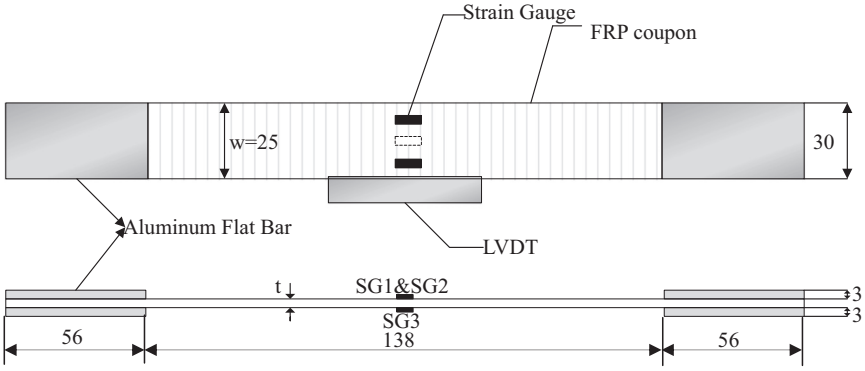

Fig. 6. Coupon details.

Table 4
FRP coupon test results.

Type of FRP	Thickness of FRP (mm)	Tensile strength (MPa)	Ultimate strain (%)	Modulus of elasticity (GPa)
GFRP	0.436	967	1.60	60.8
CFRP	0.167	3200	1.50	213

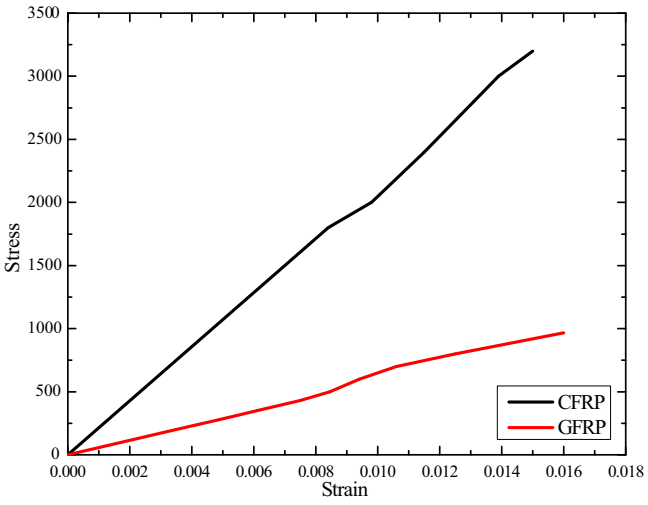

Fig. 7. Typical tensile stress-strain curves of GFRP and CFRP composites.

3.2. Compressive stress-strain behavior

The compressive stress-axial strain curves of GFRP-confined RAC-RCBA are illustrated in Fig. 9. In general, there is no distinct difference between GFRP confined NAC (i.e. the replacement ratio of RCBA is 0%) and the GFRP confined RAC-RCBA specimens, i.e. a typical bilinear axial stress-strain behavior. All the curves behaved similarly at the initial stage with a linear response where the confinement of FRP was not activated. With an increase of applied load, the concrete core started to expand laterally and the micro-cracks propagated in the concrete core. When the applied stress approached the ultimate strength of the unconfined concrete, the confinement mechanism of FRP tube was activated, hereafter the lateral pressure increased with further lateral expansion of the concrete core. In Fig. 9, the transition zone between the two linear stages was smoother for specimen with a high replacement ratio of RCBA. The second linear region was mainly dominated by

Fig. 8. Typical failure of specimens: (a) Plain RAC-RCBA, (b) GFRP-confined RAC-RCBA, (c) CFRP-confined RAC-RCBA.

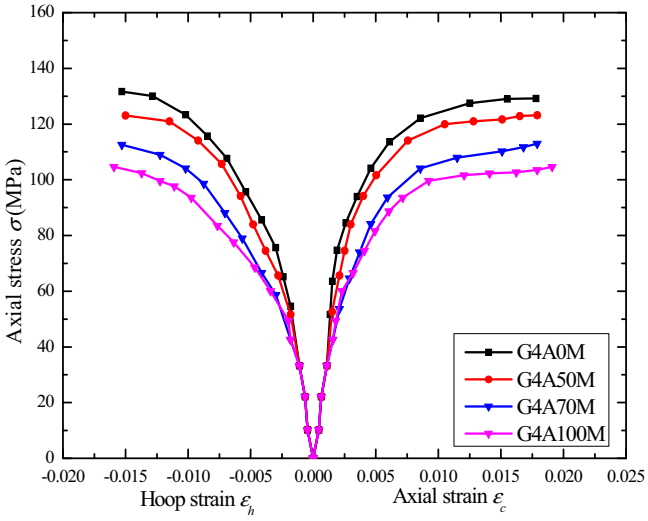

Fig. 9. Axial stress versus axial and lateral strains curves for four replacement ratios (r = 0, 50%, 70%, 100%).

the FRP tube where the tube was fully activated to confine the concrete core which leading to a considerable enhancement in compressive strength and ductility until the rupture of the FRP occurred.

3.3. Compressive results

Table 5 shows the tested results of all the specimens. In this table, P_{max} is the ultimate axial load, the ultimate axial stress and strain of unconfined concrete is defined as f_{co} and ε_{co} respectively, the confinement stiffness is listed as the lateral confining pressure f_l expressed as Eq. (1) according to Lam and Teng [46], the corresponding ultimate axial stress and strain is defined as f_{cc} and ε_{cu} respectively, and the average ultimate tensile strain tested from the FRP coupon tests and the confined concrete cylinders is defined as ε_{fu} and $\varepsilon_{fu,a}$, respectively.

$$f_l = 2f_{frp}t_{frp}/d \tag{3.1}$$

Table 5 shows clearly that the ultimate compressive strength was improved significantly due to the lateral confinement of FRP, e.g. the average ultimate strength f_{cc} of PCA70M, G2A70M, G4A70M and C4A70M were 33.3 MPa, 67.0 MPa, 112.9 MPa and 137.0 MPa, respectively. It is apparent that the rupture strains were very similar for GFRP tube confined specimens with the same confinement stiffness but different replacement ratios of RCBA. The confinement effectiveness (i.e. the ratio of ultimate compressive stress of confined concrete to that of unconfined concrete (f_{cc}/f_{co}) indicates that the use of GFRP and CFRP confinement improved the compressive strength and axial strain of RAC-RCBA significantly, which increased with an increase of the tube thickness. The CFRP confinement provided larger enhancement in ultimate compressive strength but resulted in smaller ultimate axial strain. Therefore, current study showed that the CFRP tube confined RAC-RCBA provided higher enhancement in ultimate compressive strength but lower ultimate axial strain than those of GFRP tube-confined RAC-RCBA due to its higher elastic modulus and tensile strength but lower tensile strain of CFRP compared with those of GFRP. This observation is similar to that concluded by Xie and Ozbakkaloglu [43] on carbon and basalt FRP tube confined RAC, i.e. CFFTs manufactured with carbon FRP tubes instead of basalt FRP tubes develop a higher compressive strength and lower ultimate axial strain of the confined RAC, where the tensile modulus and strength of CFRP are significantly larger but the tensile strain is lower than those of basalt FRP.

Obviously, the rupture strains of the FRP tubes were smaller than those obtained from the flat coupon tensile tests, the reasons can be attributed to: (a) the ignorance of axial compressive

Table 5
Experimental data.

Specimens	r (%)	FRP	n_f	f_l (MPa)	f_{co} (MPa)	f_l/f_{co}	ε_{co} (%)	ε_{fu} (%)	P_{max} (kN)	f_{cc} (MPa)	f_{cc}/f_{co}	ε_{cu} (%)	$\varepsilon_{fu,a}$ (%)
G4A0M	0	G	4	23.95	35.86	0.67	0.26	1.60	1033.69	129.21	3.63	1.78	1.41
G4A50M	50	G	4	23.95	35.55	0.66	0.27	1.60	1012.97	123.20	3.47	1.79	1.41
G4A100M	100	G	4	23.95	31.73	0.70	0.30	1.60	862.60	104.67	3.30	1.91	1.41
G4A70M	70	G	4	23.95	33.27	0.67	0.28	1.60	962.47	112.93	3.39	1.86	1.41
G6A70M	70	G	6	33.32	33.27	1.00	0.28	1.60	1307.47	148.59	4.47	2.28	1.53
G2A70M	70	G	2	9.28	33.27	0.28	0.28	1.60	552.67	66.99	2.01	1.51	1.31
C2A70M	70	C	2	12.41	33.27	0.37	0.28	1.50	651.10	96.16	2.89	1.41	0.98
C4A70M	70	C	4	27.79	33.27	0.84	0.28	1.50	1133.89	136.99	4.12	1.62	0.76
C6A70M	70	C	6	40.73	33.27	1.22	0.28	1.50	1540.33	161.26	4.85	1.71	0.64

contribution of the FRP tube, (b) the easier fabrication of flat coupons lead to higher quality than FRP tubes, (c) the complex interaction between the FRP tube and concrete, and (d) the non-uniform deformation of cracked concrete.

3.3.1. Influence factors on properties of FRP-confined RAC-RCBA

Three influent factors were considered in the experiment, i.e., the replacement ratio of RCBA r, the confinement stiffness of FRP tube t_{frp}, and the type of FRP materials (GFRP and CFRP). The three replacement ratios of RCBAs were $r = 50\%$, 70% and 100% compared with the confined NAC. In the Fig. 9, the GFRP-confined RAC-RCBA, G4A50M, G4A70M and G4A100M behaved a similar linear stress-strain behavior to that of the G4A0M (NAC) at the first linear stage, while the slopes of the second linear stage for specimens with a smaller replacement ratio was larger which resulted in a larger ultimate compressive stress. With a larger replacement ratio of RCBA, the ultimate compressive stress of the confined specimen decreased lightly, but the FRP-confined RAC-RCBA still performed well in strain development. While in general, the stress-strain behavior of the confined-specimens shows insignificant difference for specimens with different replacement ratios of RCBA, as illustrated in Fig. 9. As listed in Table 5, the ultimate compressive strength of both CFRP and GFRP tube confined RAC-RCBA specimens decreased with an increase in RCBA replacement ratio due to the decrease of hoop rupture strains $\varepsilon_{h,rup}$. The ultimate axial strain of both GFRP and CFRP tube confined RAC-RCBA increased slightly with an increase of RCBA replacement ratio, while the axial strain enhancement ratio ($\varepsilon_{cu}/\varepsilon_{co}$) decreased, e.g. the ultimate axial strain ε_{cu} of G4A0M, G4A50M, G4A70M and G4A100M is 1.78%, 1.79%, 1.86% and 1.91%, while the axial strain enhancement ratio ($\varepsilon_{cu}/\varepsilon_{co}$) is 6.84, 6.63, 6.43 and 6.36, which indicates that the effect of RA replacement ratio on the dilation of FRP tube confined RAC-RCBA is similar to FRP-confined RAC reported by Zhao et al. [42] and Xie and Ozbakkaloglu [43].

The effects of confinement stiffness (number of FRP layers) and type of FRP materials on the compressive stress-strain behavior of confined RAC-RCBA are shown in Fig. 10. Like the FRP-confined NAC, the ultimate stress of the specimen increased with a larger tube thickness and so did the slope of the second linear stage, hence the confined RAC-RCBA with a larger tube thickness failed with a higher stress but similar ultimate axial strain. Based on the current tested results, the average ratio $\varepsilon_{fu,a}/\varepsilon_{fu}$ increased with an increase in the number of FRP layers (Table 5), e.g. the average ratio $\varepsilon_{fu,a}/\varepsilon_{fu}$ was 0.81, 0.88 and 0.95 for G2A70M, G4A70M and G6A70M, respectively. The CFRP-confined specimens had a higher ultimate strength than the corresponding GFRP-confined specimen and the increment of strength decreased with a higher FRP stiffness, e.g., the average increments of C2A70M to G2A70M, C4A70M to G4A70M and C6A70M to G6A70M correspond to 29.2 MPa, 24.1 MPa and 12.7 MPa, respectively, and the stress-strain curves behaved quite similar, but the ultimate axial strains were lower.

3.3.2. Dilation behavior

Dilation behavior of FRP-confined RAC-RCBA is discussed here. When the applied axial stress was close to or exceeded the ultimate strength of the unconfined concrete, the outer FRP tube was activated to confine the concrete core which initiated dilation of the confined concrete. Figs. 9 and 10 present the axial stress-lateral strain curves due to dilation effects measured on the specimens with different RCBA replacement ratios, FRP stiffness and fibre materials. Fig. 9 illustrates that the dilation is significantly larger in confined RAC-RCBA than that in the confined NAC (i.e. with RA replacement ratio of 0).

The dilation rate (μ_t) expressed as the slope of the lateral strain increment to axial strain increment is given by Eq. (3.2) [47] and the corresponding dilation rate of GFRP and CFRP confined RAC-RCBA is presented in Fig. 11.

$$\mu_t = \Delta\varepsilon_h/\Delta\varepsilon_c \tag{3.2}$$

As illustrated in Fig. 11, the ultimate axial strain increases with an increase of FRP confinement, while the increase in RCBA content decreases the dilation rate of the tube confined concrete with contributions from the decreased hoop strain and increased axial strain, the peak dilation rate of the GFRP tube confined specimen under loads is higher than that of CFRP tube confined specimens, and the GFRP-confined specimens show better axial strain gain than the CFRP-confined specimens due to the larger tensile strain and lower tensile modulus of GFRP materials.

3.3.3. Confinement ratio

Confinement ratio is defined as f_l/f_{co} to evaluate the effectiveness of confinement. The lateral pressures f_l of 2, 4 and 6 layers GFRP tube confined RAC-RCBA (RCBA replacement ratio of 70%) are 9.3 MPa, 24.0 MPa and 33.3 MPa, respectively, those of 2, 4 and 6 layers CFRP tube confined RAC-RCBA (RCBA replacement

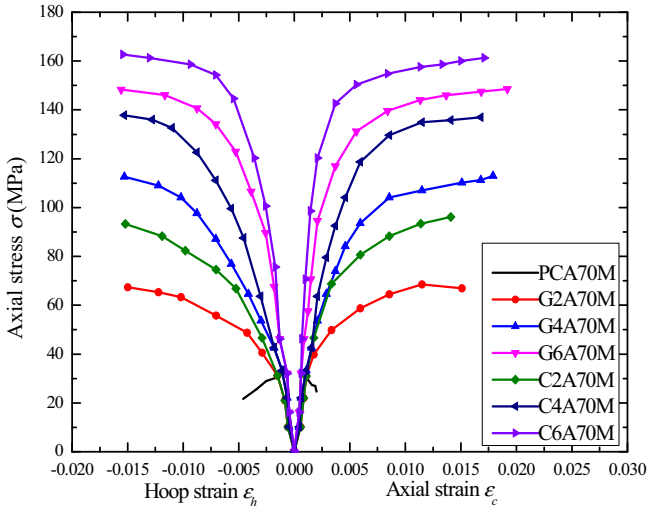

Fig. 10. Axial stress versus axial and lateral strains curves for 2, 4 and 6 layers GFRP and CFRP confined RAC specimens.

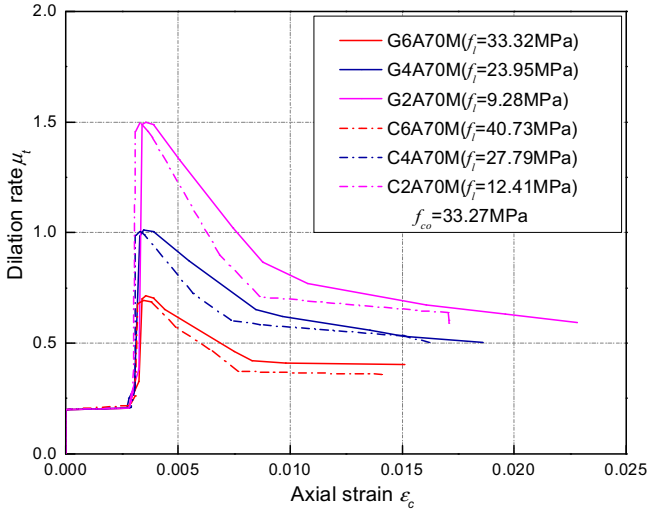

Fig. 11. Dilation rates of GFRP and CFRP-confined specimens with different layers of 2, 4 and 6.

ratio of 70%) are 12.4 MPa, 27.8 MPa and 40.7 MPa, respectively, calculated as $f_l = 2f_{frp}t_{frp}/d$ and the confinement ratios were calculated and given in Table 5. According to Spoelstra and Monti [48], an effective confinement of FRP confined concrete means the confinement ratio of the specimen is beyond 0.07, thus, it can be concluded that all the G/CFRP tube confined RCA-RCBA specimens in this study exhibited effective confinement.

4. Confinement models

Ozbakkaloglu et al. [32] reviewed over 80 stress-strain models developed for FRP-confined circular NAC and the models with best prediction accuracy were evaluated and recommended. Thus, the experimental results of current study were compared with the predicted values using the five of the best performing design-oriented models and two of the best performing analysis-oriented models which recommended by Ozbakkaloglu et al. [32] for FRP-confined NAC, i.e. design-oriented models by Teng et al. [49,50], Moran and Pantelides [51], Lam and Teng [52], Bisby et al. [53] and Ozbakkaloglu and Jim [54], and three analysis-oriented models by Teng et al. [54] and Mander at al. [55] based on the expressions developed by Richart et al. [56]. The design-oriented models are more accurate for the predictions of the ultimate strength and strain enhancement ratios in general and all the analysis-oriented models were explicitly derived from FRP-confined and actively confined concrete dilation relationships which perform better than those from implicitly adopted dilation relationships [32]. Both Teng's models [49,50] took FRP hoop strain reduction into account. The design-oriented models expressed as a linear relationship of strength-to-lateral confining pressure were expressed as Eq. (4.1) by Moran and Pantelides [51], Eq. (4.2) by Lam and Teng [52] and Eq. (4.3) by Bisby et al. [53], where f_{lu} is the ultimate lateral confining pressure.

$$\frac{f_{cc}}{f_{co}} = 1 + k_1\frac{f_{lu}}{f_{co}} \tag{4.1}$$

k_1 = 4.1 for bonded FRP shell k_1 = 2.33 for unbounded FRP shell

$$\frac{f_{cc}}{f_{co}} = 1 + 3.3\frac{f_{lu}}{f_{co}} \tag{4.2}$$

$$\frac{f_{cc}}{f_{co}} = 1 + 2.425\frac{f_{lu}}{f_{co}} \tag{4.3}$$

One most recently developed model by Ozbakkaloglu and Lim [54] was expressed as Eqs. (4.4) series which was developed based on a comprehensive and accurate study of FRP-confined concrete experimental database, where f_{l0} is the threshold confining pressure, $f_{lu,a}$ is the reduced actual confining pressure, f_{cl} is the first peak stress, k_1 is the coefficient of strength enhancement, K_l is the confinement stiffness.

$$f_{cc} = c_1 f_{co} + k_1(f_{lu,a} - f_{l0}) \tag{4.4}$$

$$c_1 = \frac{f_{c1}}{f_{co}} = 1 + 0.0058\frac{K_l}{f_{co}} \tag{4.4.1}$$

$$f_{l0} = K_l\varepsilon_{l1} \tag{4.4.2}$$

$$\varepsilon_{l1} = \left(0.43 + 0.009\frac{K_l}{f_{co}}\right)\varepsilon_{co} \tag{4.4.3}$$

$$K_l = \frac{2E_f t_f}{D} \text{ and } K_l \geqslant f_{co}^{1.65} \tag{4.4.4}$$

The strength model and one strain model by Teng et al. [49,50] were expressed as Eqs. (4.5) and (4.6), the strength models consist of the first parabolic part and the second linear part, where E_{c1} is the elastic modulus of unconfined concrete, E_{c2} is the slope of the second linear portion, ε_{c1} is the transition strain at where the two stages connect smoothly, ε_{cu} is the ultimate axial strain. In the strain model, the confinement stiffness ratio ρ_K and strain ratio ρ_ε are expressed as Eqs. (4.6.1) and (4.6.2), the $\varepsilon_{h,rup}$ is the hoop rupture strain of FRP.

$$\begin{cases} \frac{f_{cc}}{f_{co}} = E_{c1}\varepsilon_c - \frac{(E_{c1}-E_{c2})^2}{4f_{co}}\varepsilon_c^2 & \text{for } 0 \leqslant \varepsilon_c \leqslant \varepsilon_{c1} \\ \frac{f_{cc}}{f_{co}} = f_{co} - E_{c2}\varepsilon_c & \text{for } \varepsilon_{c1} \leqslant \varepsilon_c \leqslant \varepsilon_{cu} \end{cases} \tag{4.5}$$

$$\varepsilon_{c1} = \frac{2f_{co}}{E_{c1} - E_{c2}} \tag{4.5.1}$$

$$\varepsilon_{c2} = \frac{f_{cc} - f_{co}}{\varepsilon_{cu}} \tag{4.5.2}$$

$$\frac{\varepsilon_{cc}}{\varepsilon_{co}} = 1.75 + 6.5\rho_K^{0.8}\rho_\varepsilon^{1.45} \tag{4.6}$$

$$\rho_K = \frac{E_{frp}t_{frp}}{f_{co}d/\varepsilon_{co}} \tag{4.6.1}$$

$$\rho_\varepsilon = \varepsilon_{h,rup}/\varepsilon_{co} \tag{4.6.2}$$

The analysis-oriented models presented in a linear way by Teng et al. [54] and the most commonly used ultimate stress expression given by Mander at al. [55] expressed as following Eq. (4.7) and (4.8). The most commonly used strain expression was the one originally proposed by Richart et al. [56]. The models were considered through comparisons with independent test data, and were a widely applicable lateral strain equation based on a careful interpretation of the lateral deformation characteristics of unconfined, actively confined and FRP-confined concrete.

$$\frac{f_{cc}}{f_{co}} = 1 + 3.5\frac{f_l}{f_{co}} \tag{4.7}$$

$$\frac{f_{cc}}{f_{co}} = 2.254\sqrt{1 + \frac{7.94f_l}{f_{co}}} - 2\frac{f_{lu}}{f_{co}} + 1.254 \tag{4.8}$$

$$\varepsilon_{cc} = 5\varepsilon_{co}\left(\frac{f_{cc}}{f_{co}} - 0.8\right) \tag{4.9}$$

Based on the models above, the comparisons between predicted values based on these models and the experimental results obtained from this study are illustrated in Figs. 12–14, each series of specimens have three tested ultimate compressive strength and axial strain listed in the curves, and the mean value and the coefficient of variation (COV) are showed at the left corner. It is clear that all the models provide accurate predictions for GFRP-confined and CFRP-confined RAC-RCBA specimens, especially for the ultimate compressive stress but the analysis-oriented models developed by Mander at al. [55] overestimated the ultimate strain values slightly, and the predicted values from most models are generally similar. Most design-oriented models show more accurate predictions than the analysis-oriented models with the ratio of the predicted values to the tested values which are even less than "1", and the strength models by Teng et al. [49,50] and Ozbakkaloglu and Lim [54] performed better, while the design-oriented model by Moran and Pantelides [51] predicted the ultimate strength a little conservative. However, the effect of replacement ratio of RCBAs should be incorporated into the development of models, especially for modeling the ultimate axial strain, thus, more accurate confinement models should be developed for FRP confined RAC with RCBA and more experimental works on FRP confined RAC-RCBA considering more experimental parameters are needed.

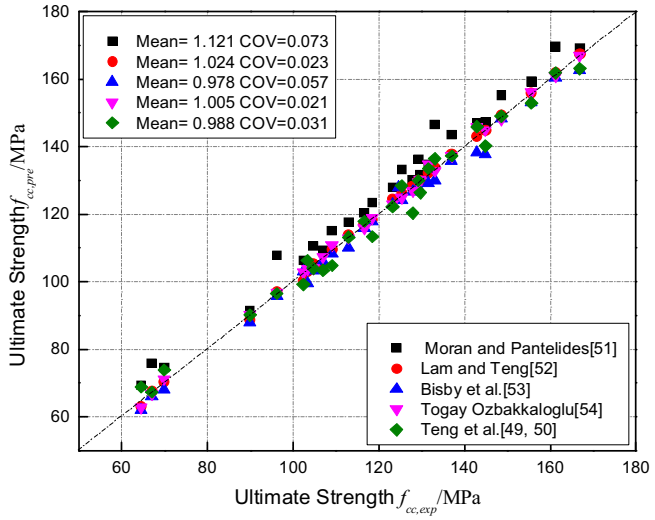

Fig. 12. Performance of design-oriented models: ultimate axial stress.

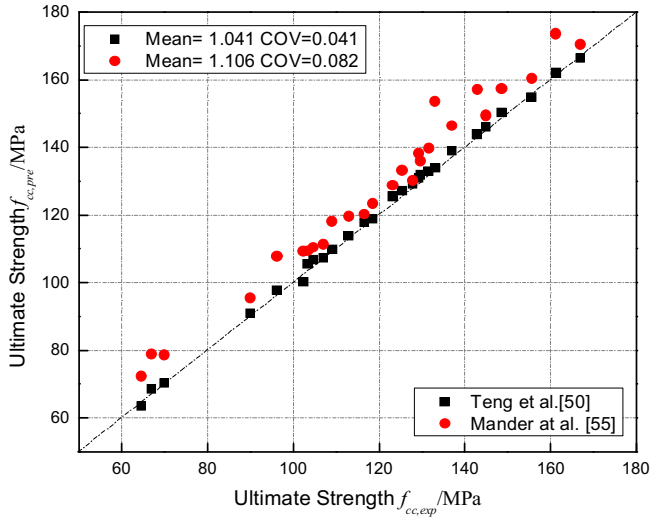

Fig. 13. Performance of design-oriented models: axial strain at ultimate stress.

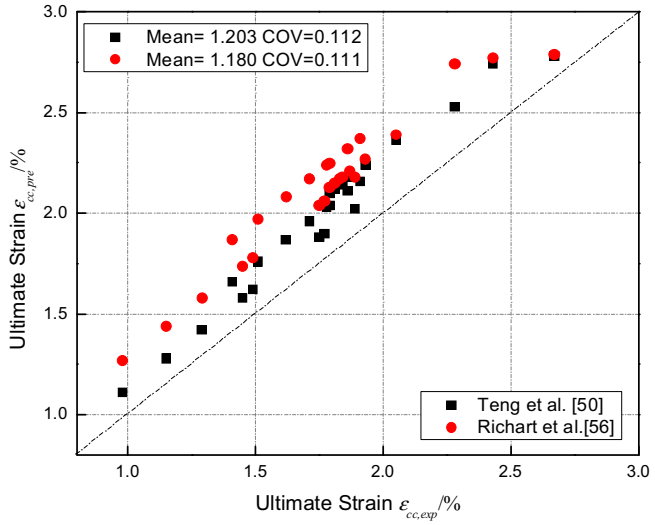

Fig. 14. Performance of design-oriented and analysis-oriented models: axial strain at ultimate stress.

5. Conclusion

This study was the first systematic study which considered the compressive behavior of FRP-confined recycled aggregate concrete (RAC) with recycled clay brick aggregate (RCBA). Experimental parameters such as the replacement ratio of RCBA, FRP stiffness, and the type of FRP were investigated. Several existing confinement models for FRP-confined NAC were used to model the behavior of FRP confined RAC-RCBA. The following conclusions can be drawn:

1. Like the normal RAC with recycled aggregates from old concrete components, an increase in replacement ratio of RCBA reduces the compressive strength of RAC-RCBA cylinders and the dilation rate, but slightly increases the axial strain, however there was no obvious effect on the compressive strength when the replacement ratio of RCBA was beyond 70%.
2. The confinement of either GFRP or CFRP tube improved the compressive behavior of RAC-RCBA remarkably, i.e. the ultimate compressive strength of confined RAC-RCBA with RCBA replacement ratio of 70% increased almost 5.5 times by 6-layer GFRP tube confinement. But carbon FRP tube confined RAC-RCBA exhibited lower ultimate axial strain and higher compressive strength compared with that of glass FRP tube confined RAC-RCBA.
3. The general compressive behavior of carbon or glass FRP-confined RAC-RCBA was similar to that of FRP-confined NAC, while the slopes of the second stage at the axial stress-strain curves exhibit cycloidal trend with an increase of RCBA replacement ratio.
4. The dilation is significantly higher in FRP-confined RAC-RCBA than that in confined NAC, and an increase in RCBA replacement ratio decreases the dilation rate of the confined RAC-RCBA due to the decreased hoop strain and increased axial strain. The peak dilation rate of GFRP-confined RAC-RCBA is higher than that of the CFRP confined specimens due to its higher ultimate elongation and lower tensile modulus of glass FRP materials.
5. The design-oriented and analysis-oriented models recommended by Ozbakkaloglu et al. [32] for FRP-confined NAC provided accurate predictions on the ultimate compressive stress of FRP tube confined RAC-RCBA, while the strain models slightly exaggerated the ultimate axial strain and the analysis-oriented models was a little conservative. The models developed by Teng et al. [49,50] and Ozbakkaloglu and Lim [54] exhibited better performance in predicting the compressive strength of FRP tube confined RAC-RCBA.

Acknowledgement

The research was funded by the Natural Sciences Foundation of Hunan Province, China (Grant No. 2015JJ3032). The authors appreciate the support received from Master G.M. Gu, B. Yan and L.X. Chen.

References

[1] Torring M, Lauritzen E. Total recycling opportunities-tasting the topics for the conference session. In: Dhir RK, Dyer TD, Halliday JE, editors. Proc., int. congress: challenges of concrete construction, conf. 2-sustainable concrete construction. London: Thomas Telford Publishing; 2002. p. 501–10.
[2] Tang P, Yang P. Analysis of industrialization of C&D waste disposition in China. Jiangsu Constr 2007;3:57–60.
[3] Xiao JZ. Recycled concrete. Beijing, China: China Architecture & Building Press; 2008.
[4] Mohammed Tarek Uddin, Hasnat Ariful, Awal Mohammad Abdul, Bosunia Shamim Z. Recycling of brick aggregate concrete as coarse aggregate. J Mater Civ Eng 2015;27(7):B4014005.

[5] Buck AD. Recycled concrete as a source of aggregate. ACI J 1977;74:212–9.
[6] Hansen TC. Recycling of demolished concrete and masonry. London: E&FN Spon; 1992.
[7] Watson K. Rocky road to recycling. Surveyor 1993;180:17–8.
[8] Collins RJ, Sherwood PT. Use of waste and recycled materials as aggregates: Specifications and standards. HMSO, London: Dept. of the Environment Rep; 1995.
[9] Khalaf FM, De Venny AS. Recycling of demolished masonry rubble as coarse aggregate in concrete: review. J Mater Civ Eng 2004;164:331–40.
[10] Khalaf FouadM, De Venny AlanS. Properties of new and recycled clay brick aggregates for use in concrete. J Mater Civ Eng 2005;17(4):456–64.
[11] Municipality of Mashhad. Annual report of construction and demolition debris. Technical Rep. No. RTMO-85, Research Centre for Mashhad City Council, Mashhad, Iran; 2007.
[12] Jin WL, Yue ZG, Gao LY. State-of-the-art development on code for design of masonry structures. J Build Struct 2010;31(6):22–8.
[13] Wahlstrom M, Laine YJ, Maattanen A, Luotojarvi T, Kivekas L. Environmental assurance system for use of crushed mineral demolition waste in road construction. Waste Manage 2000;20(2):225–32.
[14] Yang J, Du Q, Bao YW. Concrete with recycled concrete aggregate and crushed clay bricks. Constr Build Mater 2011;26:1935–45.
[15] Khalaf Fouad M. Using crushed clay brick as coarse aggregate in concrete. J Mater Civ Eng 2006;18(4):518–26.
[16] Poon CS, Kou SC, Lam L. Use of recycled aggregated in moulded concrete bricks and blocks. Constr Build Mater 2002;32:281–9.
[17] Bazaz Jafar Bolouri, Khayati Mahmood. Properties and performance of concrete made with recycled low-quality crushed brick. J Mater Civ Eng 2012;24 (4):330–8.
[18] Park C, Sim J. Fundamental properties of concrete using recycled concrete aggregate produced through advanced recycling process. Transportation research board 85th annual meeting, Washington, DC, USA; 2006, p. 22–6.
[19] Goncalves A, Esteves A, Vieira M. Influence of recycled concrete aggregates on concrete durability. In: RILEM proceedings PRO 40: use of recycled materials in buildings and structures; 2004.
[20] Yang YF, Han LH. Experimental behavior of recycled aggregate concrete filled steel tubular columns. J Constr Steel Res 2006;62(12):1310–24.
[21] Huang L, Yin P, Yan L, Kasal B. Behavior of hybrid GFRP-perforated-steel tube encased concrete under uniaxial compression. Compos Struct 2016;142:569–78.
[22] Gao C, Huang L, Yan L, Ma G, Xu L. Compressive behavior of CFFT with inner steel wire mesh. Compos Struct 2015;133:322–30.
[23] Huang L, Xun X, Yan L, Zhu D. Compressive behavior of concrete confined with GFRP tubes and steel spirals. Polymers 2015;7(5):851–75.
[24] Yin P, Huang L, Yan L, Zhu D. Compressive behavior of concrete confined by CFRP and transverse spiral reinforcement. Part A: experimental study. Mater Struct 2016;49(3):1001–11.
[25] Yan LB. Plain concrete cylinders and beams externally strengthened with natural flax fabric reinforced epoxy composites. Mater Struct 2015. http://dx.doi.org/10.1617/s11527-015-0635-1.
[26] Yan LB, Chouw N. Natural FRP tube confined fibre reinforced concrete under pure axial compression: A comparison with glass/carbon FRP. Thin-walled Struct 2014;82:159–69.
[27] Huang L, Gao C, Yan LB, Kasal B, Ma G. Reliability assessment of confinement models of carbon fiber reinforced polymer-confined concrete. J Reinf Plast Compos 2016;35(12):996–1026.
[28] Huang L, Gao C, Yan LB, Kasal B, Ma G. Confinement models of GFRP-confined concrete: statistical analysis and unified stress-strain models. J Reinf Plast Compos 2016;35(11):867–91.
[29] Yan LB, Chouw N, Jayaraman K. Effect of column parameters on flax FRP confined coir fibre reinforced concrete. Constr Build Mater 2014;55:299–312.
[30] Ozbakkaloglu T, Oehlers DJ. Concrete-filled square and rectangular FRP tubes under axial compression. J Compos Constr 2008;12(4):469–77.
[31] Ozbakkaloglu T, Lim JC, Vincent T. FRP-confined concrete in circular sections: Review and assessment of stress-strain models. Eng Struct 2013;49:1068–88.
[32] Vincent T, Ozbakkaloglu T. Influence of concrete strength and confinement method on axial compressive behavior of FRP confined high and ultra-high strength concrete. Compos Part B 2013;50:413–28.
[33] Ozbakkaloglu T, Vincent T. Axial compressive behavior of circular high-strength concrete-filled FRP tubes. J Compos Constr 2013;18(2):04013037.
[34] Vincent T, Ozbakkaloglu T. Influence of slenderness on stress-strain behavior of concrete filled FRP tubes: experimental study. J Compos Constr 2014;19 (1):04014029.
[35] Lim JC, Ozbakkaloglu T. Influence of silica fume on stress-strain behavior of FRP-confined HSC. Constr Build Mater 2014;63:11–24.
[36] Vincent T, Ozbakkaloglu T. Influence of fibre type on behavior of HSC-filled FRP tubes under concentric compression. Appl Mech Mater 2014;438:240–5.
[37] Vincent T, Ozbakkaloglu T. Influence of overlap configuration on the compressive behavior of CFRP confined normal-and high-strength concrete. Mater Struct 2015:1–24.
[38] Vincent T, Ozbakkaloglu T. Influence of fibre orientation and specimen end condition on axial compressive behavior of FRP confined concrete. Constr Build Mater 2015;47:814–26.
[39] Ozbakkaloglu T. Behavior of square and rectangular ulta high-strength concrete-filled FRP tubes under axial compression. Compos B 2015;54:97–111.
[40] Islam MM, Choudhury MSI, Abdulla M, Amin AFMS. Confinement effect of fiber reinforced polymer wraps in circular and square concrete columns. In: 4th annual paper meet and 1st civil engineering congress, the Institution of Engineers (IEB), Dhaka, Bangladesh; 2011. p. 359–62.
[41] Xiao JZ, Huang YJ, Yang J, Zhang C. Mechanical properties of confined recycled aggregate concrete under axial compression. Constr Build Mater 2012;26 (1):591–603.
[42] Zhao JL, Yu T, Teng JG. Stress-strain behavior of frp-confined recycled aggregate concrete. J Compos Constr 2015;19(3):04014054.
[43] Xie T, Ozbakkaloglu T. Behavior of recycled aggregate concrete-filled basalt and carbon FRP tubes. Constr Build Mater 2016;105:132–43.
[44] Standard for test method of mechanical properties on ordinary concrete (GB/T50081-2002). China Association for Engineering Construction Standardization. China Architecture & Building Press; 2002.
[45] ASTM D3039. Standard test method for tensile properties of polymer matrix composite materials. West Conshohocken, Pa, USA; 2008b.
[46] Lam L, Teng JG. Ultimate condition of fiber reinforced polymer-confined concrete. J Compos Constr 2004;8(6):539–48.
[47] Lim J, Ozbakkaloglu T. Lateral strain-to-axial strain relationship of confined concrete. Eng Struct 2015;141(5):04014141.
[48] Spoelstra MR, Monti G. FRP-confined concrete model. J Struct Eng 1999;9 (4):143–50.
[49] Teng JG, Jiang T, Lam L, Luo Y. Refinement of a design-oriented stress-strain model for FRP-confined concrete. J Compos Constr 2009;13(4):269–78.
[50] Teng JG, Huang YL, Lam L, Ye L. Theoretical model for fiber reinforced polymer-confined concrete. J Compos Constr 2007;11(2):201–10.
[51] Moran DA, Pantelides CP. Variable strain ductility ratio for fiber reinforced polymer-confined concrete. ASCE J Compos Constr 2002;6(4):224–32.
[52] Lam L, Teng JG. Design-oriented stress-strain model for FRP-confined concrete. Constr Build Mater 2003;17(6–7):471–89.
[53] Bisby LA, Dent AJS, Green MF. Comparison of confinement models for fiber-reinforced polymer-wrapped concrete. ACI Struct 2005;102(1):62–72.
[54] Ozbakkaloglu T, Lim JC. Axial compressive behavior of FRP-confined concrete: experimental test database and a new design-oriented model. Compos B 2013;55:607–34.
[55] Mander JB, Priestley MJN, Park R. Theoretical stress–strain model for confined concrete. Eng Struct 1988;114(8):1804–26.
[56] Richart FE, Brandtzaeg A, Brown RL. A study of the failure of concrete under combined compressive stresses. In: Bulletin no. 185, Univ. of Illinois, Eng. Experimental Station: Champaign, Ill; 1928.